

基于多光混频的方法产生平坦毫米波噪声

陈永祥, 刘文杰, 孙粤辉, Romain Zinsou, 王云才*

广东工业大学信息工程学院广东省信息光子技术重点实验室, 广东 广州 510006

摘要 提出了一种基于多光混频产生平坦毫米波噪声的方法。通过宽带放大自发辐射(ASE)光源, 滤出多个具有不同中心波长的高斯型噪声光谱, 利用宽带光电探测器, 对多个具有不同中心波长的噪声光谱进行了混频以产生平坦毫米波噪声。仿真结果表明, 所提方案能够在高频率范围内产生平坦的毫米波噪声, 如 F 波段(90~140 GHz)和 G 波段(140~220 GHz)。为了定量地比较毫米波噪声的质量, 定义了相对平坦度为某个频率范围内产生噪声功率的起伏与其平均功率之比。实验结果表明, 产生的毫米波噪声的相对平坦度低至 0.46[@(35±15)GHz]。

关键词 光学仪器; 平坦度; 毫米波噪声; 多光混频; 光电转换

中图分类号 TN29

文献标志码 A

doi: 10.3788/CJL202249.0714001

1 引言

噪声发生器已被广泛应用于雷达系统^[1]、气体传感^[2]、通信系统^[3]、无损成像^[4]和辐射计校准^[5]等领域。噪声功率谱的平坦度是衡量噪声发生器性能的重要参数之一。噪声功率谱的不平坦性会严重制约噪声发生器的应用, 例如, 在测量器件的噪声系数时, 功率谱不平坦的毫米波噪声会增加噪声系数分析仪的噪声功率测量范围, 进而降低噪声系数的动态精度^[6]。

目前报道的噪声发生器主要是基于电学的方法实现的^[7-9], 但受工作带宽的限制, 利用该方法产生的毫米波噪声功率会随着频率的增加而下降, 从而导致产生不平坦的噪声功率谱。相比于电学的方法, 利用光学方法更容易获得宽频率范围的毫米波噪声, 例如利用宽带放大自发辐射(ASE)噪声的光电转换产生宽频的毫米波噪声。此外, 已有报道也指出, 输出电噪声的频谱形状与输入噪声光谱的形状存在密切关系。1989年, Olsson^[10]从理论上证明了矩形噪声光谱经光电转换产生的频谱噪声为三角形。2007年, Duan等^[11]数值上验证了洛伦兹形状的噪声光谱经光电转换产生了洛伦兹形状的频谱噪

声。2008年, Song等^[12]通过理论和实验证明, 利用阵列波导光栅和宽带 ASE 光源滤出的高斯型噪声光谱经单行载流子光电探测器光电转换后, 产生了高斯型的频谱噪声。但据我们所知, 还没有一种光学的方法来产生具有均匀功率分布的平坦毫米波噪声。

为了解决上述功率谱不平坦的问题, 本文提出了一种基于多光混频产生平坦毫米波噪声的方法。通过控制滤波后光谱的半峰全宽(FWHM)及中心波长, 可获得合适的光功率, 进而确保产生较大的噪声功率。为了证明所提方法的有效性, 本文开展了原理性实验验证和数值仿真。实验结果表明, 所产生的毫米波噪声的相对平坦度(η)低至 0.46[@(35±15)GHz]。另外, 数值仿真结果与实验结果高度一致, 进一步证明了该方法的有效性。当不受光电探测器带宽的限制时, 该方法能够获得更宽频率范围的平坦毫米波噪声。因此, 所提出的多光混频方法在产生平坦毫米波噪声方面具有良好的应用潜力。

2 基本原理

本节主要介绍利用多光混频产生平坦毫米波噪声的基本原理。目前, 光子毫米波噪声主要是

收稿日期: 2021-07-06; 修回日期: 2021-08-14; 录用日期: 2021-09-06

基金项目: 国家自然科学基金(61927811, 61961136002, 61731014)

通信作者: *wangyc@gdut.edu.cn

利用两个不同波长噪声的光谱,通过混频的方法产生,所产生的频谱噪声主要集中在毫米波频率区域^[13]。然而,该方法输出的电噪声的频谱形状取决于噪声光谱的形状(如高斯型),从而导致产

生的电噪声功率谱不平坦,如图 1(a)所示。此外,噪声光谱具有较宽的半峰全宽,会导致光电探测器过饱和及较差的频率响应,进而导致输出噪声功率过低^[14]。

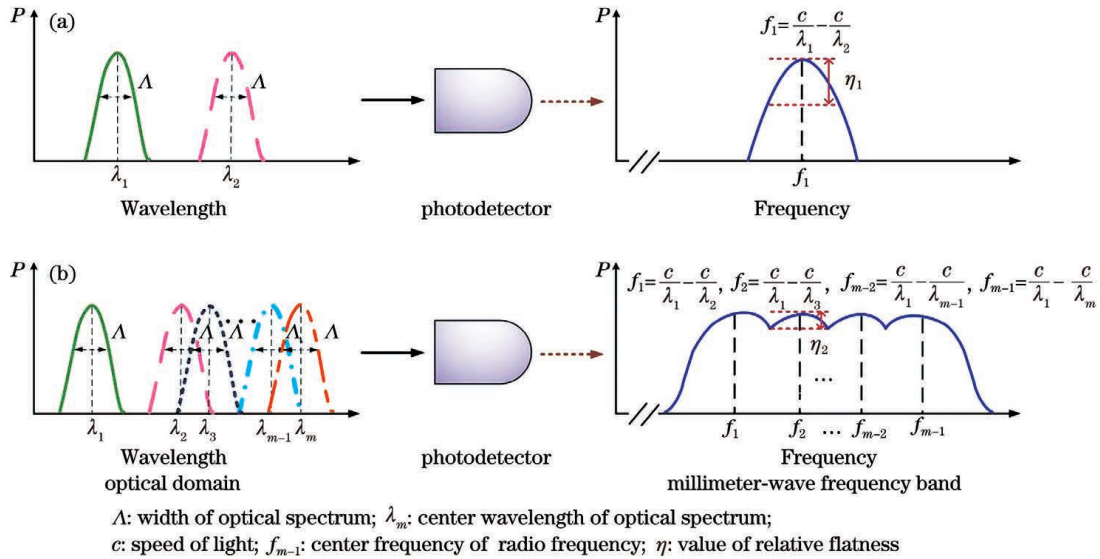


图 1 毫米波噪声产生的原理示意图。(a)两个高斯型噪声光谱的混频;(b)多个高斯型噪声光谱的混频

Fig. 1 Schematics of generation of millimeter-wave noise. (a) Optical mixing of two Gaussian noise spectra; (b) optical mixing of multiple Gaussian noise spectra

图 1(b)所示为利用多光混频方法提高电噪声功率谱平坦度的原理示意图。首先,利用光滤波器^[15]从宽带 ASE 光源^[16]中滤出 m 个具有不同中心波长且半峰全宽较窄的高斯型噪声光谱($\lambda_1, \lambda_2, \dots, \lambda_m$)。其中,两个中心波长为 λ_1 和 λ_2 的光谱波长差($\lambda_2 - \lambda_1$)将决定产生电噪声频谱的频率 f_1 ,而电噪声频谱的频率 f_{m-1} 取决于两个中心波长为 λ_1 和 λ_m 的光谱波长差($\lambda_m - \lambda_1$)。当两个连续的光谱之间的差值($\lambda_3 - \lambda_2, \lambda_4 - \lambda_3, \dots, \lambda_m - \lambda_{m-1}$)不大于光滤波器的带宽时, m 个光谱在光电探测器中发生混频,最终产生 $f_1 \sim f_{m-1}$ 频率范围内的平坦毫米波噪声。同时,波长为 $\lambda_2, \dots, \lambda_m$ 的光谱相互混频,在直流附近的低频范围内产生电噪

声,但不在我们的目标毫米波频率范围。

假设滤波后的噪声光谱 $S_{ASE}(\nu)$ 为高斯型,且具有相同的光谱宽度,则其表达式^[17]为

$$S_{ASE}(\nu) = \frac{S_{ASE,0}}{m} \left\{ \exp \left[-\frac{(\nu - \nu_1)^2}{2\Delta^2} \right] + \dots + \exp \left[-\frac{(\nu - \nu_m)^2}{2\Delta^2} \right] \right\}, \quad (1)$$

式中: $S_{ASE,0}$ 为噪声光谱的峰值幅度; m 为滤波后的噪声光谱数量; ν 为光谱频率; ν_m 为第 m 束噪声光谱的中心频率; Δ 为噪声光谱的宽度。

光电转换产生的电噪声频谱 $S_a(f)$ 与输入噪声光谱的自相关成正比,其表达式^[17-19]为

$$S_a(f) = \frac{2kR_0 \Re^2(f) P^2}{m \sqrt{\pi} \Delta} \left\{ \frac{1}{m} \exp \left\{ -\frac{[f - (\nu_m - \nu_{m-1})]^2}{4\Delta^2} \right\} + \dots + \frac{1}{m} \exp \left\{ -\frac{[f - (\nu_m - \nu_1)]^2}{4\Delta^2} \right\} + \exp \left(-\frac{f^2}{4\Delta^2} \right) \right\}, \quad (2)$$

式中: f 为电频谱频率; k 为最大功率传输系数; R_0 为系统阻抗; $\Re(f)$ 为光电探测器的响应曲线; P 为入射平均光功率。

根据多光混频原理和(2)式,在频率范围在 $[f_1, f_{m-1}]$ 内,所产生的电噪声的功率起伏(μ)与输入光谱的个数和光谱的线宽(Δ_{FWHM})有关,其表达式为

$$\mu = 10 \lg \left\{ \sum_{i=0}^{m-2} \exp \left\{ - \frac{|2i-1| \ln 2}{2} \left[\frac{(\nu_m - \nu_2)}{(m-2)\Delta_{FWHM}} \right]^2 \right\} \right\} - 10 \lg \left\{ 1 + \exp \left\{ - 2 \ln 2 \left[\frac{(\nu_m - \nu_2)}{(m-2)\Delta_{FWHM}} \right]^2 \right\} \right\} + \sum_{i=1}^{m-3} \exp \left\{ - 2 \ln 2 \left[\frac{i(\nu_m - \nu_2)}{(m-2)\Delta_{FWHM}} \right]^2 \right\} \right\}, \quad (3)$$

式中: $i=0, 1, \dots, m-2$; 光谱的半峰全宽 $\Delta_{FWHM} = 2\sqrt{\ln 4} \Delta$ 。

为了定量地分析产生毫米波噪声的质量, 我们在 $f_o \pm a$ 的频率范围内定义了相对平坦度, 其中 $f_o = (f_1 + f_{m-1})/2$ 和 $a \leq (f_{m-1} - f_1)/2$ 。相对平坦度的表达式为

$$\eta = \frac{\mu}{P_N}, \quad (4)$$

式中: P_N 为产生电噪声的平均功率。

与传统的频谱平坦度定义^[20]相比, 相对平坦度可以更好地表征产生噪声的功率起伏与其平均功率之间的关系。当两个生成的噪声具有相同的功率起伏时, 产生较高功率的电噪声将具有较小的相对频谱平坦度。

假设平均光功率保持不变, 根据 (3)、(4) 式, 在 F 波段内研究了输出电噪声的相对平坦度、光谱个数与其 FWHM 之间的关系, 数值仿真结果如图 2 所示。可以看出, 当光谱个数为 6 且其半峰全宽为 0.1 nm 时, 所得到的相对平坦度是最好的。

3 原理性实验与结果

在第 2 节中, 我们从原理上对多光混频产生平坦毫米波噪声的方法进行了可行性分析。本节将进行原理性实验的验证。

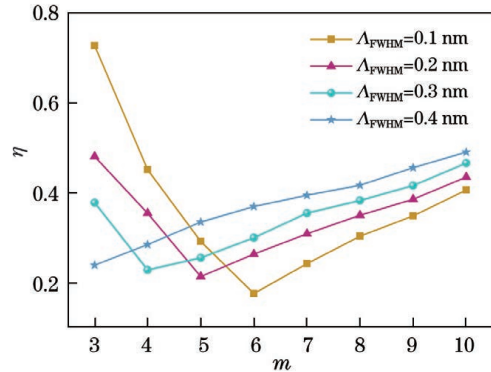


图 2 频率范围为 90~140 GHz 时不同光谱个数与 FWHM 下相对平坦度的数值仿真结果

Fig. 2 Numerical simulation results of relative flatness for different numbers of optical spectra and FWHM in frequency range of 90~140 GHz

实验装置如图 3 所示。其中, 1×4 光耦合器 (OC) 将具有 40 nm 谱宽的超辐射发光二极管 (SLD) 的光分成三路光。为了产生较高的噪声功率, 光学滤波器 (OTF) 从宽带 SLD 光源中滤出三个 3 dB 带宽为 0.1 nm 的高斯型噪声光谱, 其中中心波长分别为 $\lambda_1=1550.0$ nm, $\lambda_2=1550.2$ nm 和 $\lambda_3=1550.3$ nm。3 dB 带宽为 0.1 nm 是光学滤波器可达到的最小滤波带宽。接下来, 三个不同中心波长的高斯型噪声光谱被另一个 4×1 光耦合器耦合, 掺铒光纤放大器 (EDFA) 将耦合后的光谱功率放大到 10 mW, 继而注入到 3 dB 带宽为 50 GHz 的高速光

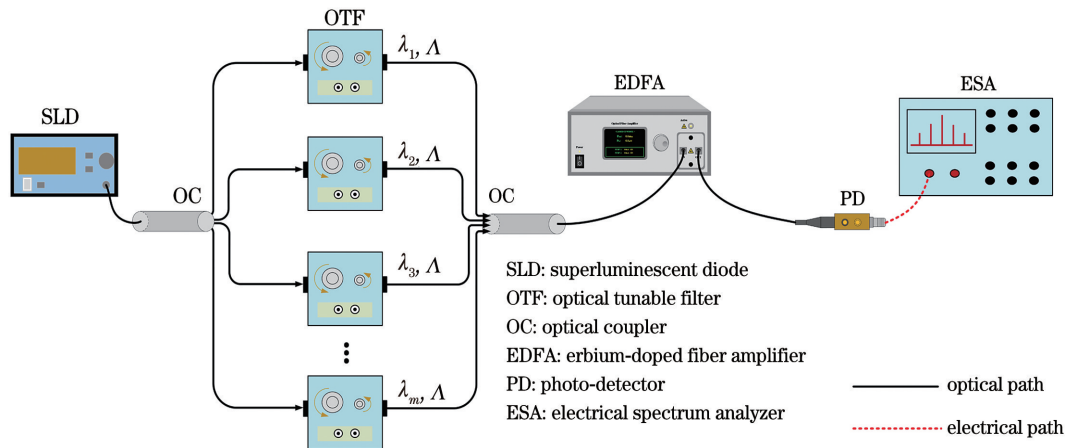


图 3 多个高斯型噪声光谱混频产生平坦毫米波噪声的实验装置图

Fig. 3 Experimental setup for generating flat millimeter-wave noise using optical mixing of multiple Gaussian noise spectra

电探测器 (PD, 光电探测器响应度 $\mathfrak{R} = 0.65 \text{ A/W}$) 中进行混频, 最后利用带宽为 50 GHz 的频谱分析仪 (ESA) 测量输出的电噪声频谱。

根据 (1)、(2) 式推导出, 当 $m = 3$ 时, 在 20 ~ 50 GHz 的频率范围内可获得平坦电噪声频谱, 图 4 所示为相关的实验结果。图 4(a) 中的曲线分别为三个经过光学滤波器滤波后的 SLD 噪声光谱

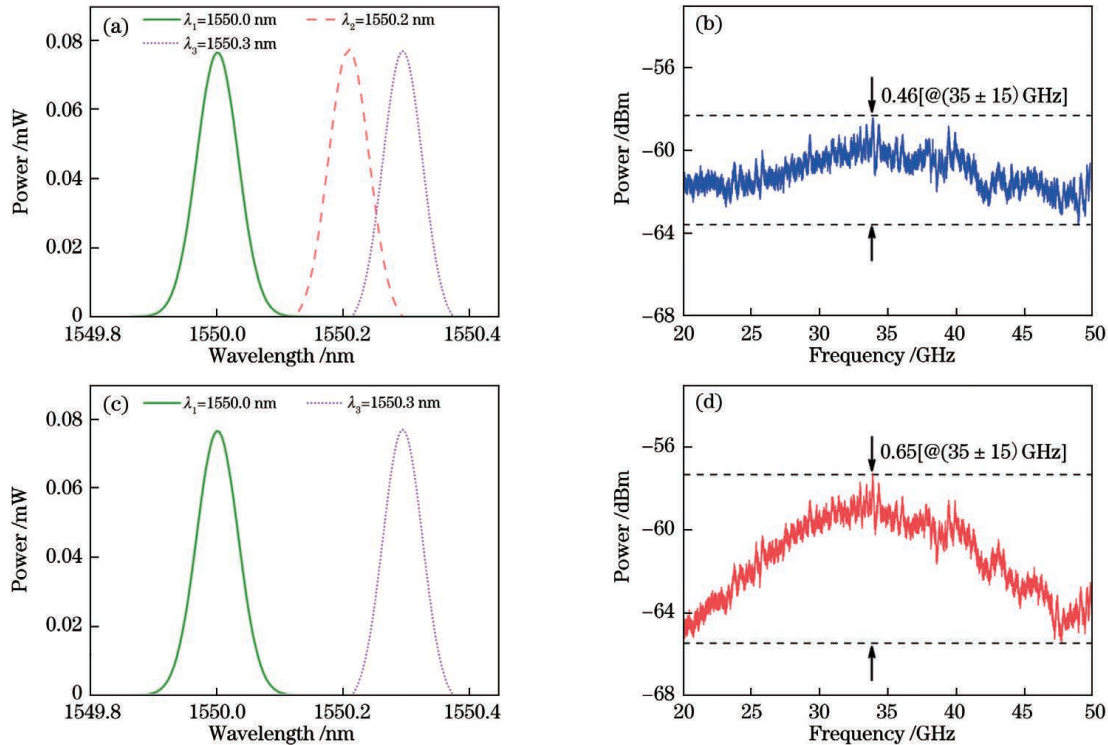


图 4 实验结果。(a) 滤波后三个高斯型噪声光谱;(b) 三光混频的频谱;(c) 滤波后两个高斯型噪声光谱;(d) 双光混频的频谱

Fig. 4 Experimental results. (a) Three Gaussian noise spectra after filtering; (b) radio frequency spectrum output from mixing of three optical spectra; (c) two Gaussian noise spectra after filtering; (d) radio frequency spectrum output from mixing of two optical spectra

作为对比, 我们进行了两个中心波长为 λ_1 和 λ_3 的高斯型噪声光谱混频产生电噪声信号的实验。原理上, 波长差为 $\lambda_3 - \lambda_1$ 的两个高斯型光谱在中心频率 37.5 GHz 处产生的高斯型电噪声频谱与实验结果基本保持一致。如图 4(d) 所示, 经过计算, 该实验所产生的电噪声的相对平坦度为 $0.65 [@(35 \pm 15) \text{ GHz}]$ 。与双光混频产生毫米波噪声的方法相比, 利用三光混频的方法获得的噪声的相对平坦度降低了 $0.19 [@(35 \pm 15) \text{ GHz}]$, 从而提升了噪声质量。

4 仿真结果

受测试设备 (如光电探测器和频谱分析仪) 的带宽限制, 我们只能在较窄的频率范围内开展验证实

验。原理上, 中心频率为 $f_1 = 25 \text{ GHz}$ 和 $f_2 = 37.5 \text{ GHz}$ 的两个高斯型电噪声频谱是由波长差为 $\lambda_2 - \lambda_1$ 和 $\lambda_3 - \lambda_1$ 的高斯型噪声光谱混频产生。因此, 如图 4(b) 所示, 平坦的毫米波噪声是由两个高斯型电噪声频谱叠加而成。实验结果表明, 在 20 ~ 50 GHz 的频率范围内, 实现了相对平坦度为 $0.46 [@(35 \pm 15) \text{ GHz}]$ 的毫米波噪声的产生。

验, 很难在较大的毫米波段和较宽的频率范围内验证所提出的方法。为了解决这个问题, 我们利用所提出的方法在 F 波段 (90 ~ 140 GHz) 进行了数值仿真, 其仿真装置如图 3 所示。谱宽为 40 nm 的 SLD 光源经光滤波器滤波后, 得到不同中心波长且半峰全宽为 0.1 nm 的高斯型噪声光谱。滤波器的 3 dB 带宽与实验保持一致。接下来, 将多个高斯型噪声光谱通过光耦合器进行耦合, EDFA 将功率放大至 10 mW 后, 将其注入到 3 dB 带宽为 90 ~ 140 GHz 的高速光电探测器 ($\mathfrak{R} = 0.4 \text{ A/W}$) 中, 最后利用带宽为 90 ~ 140 GHz 的频谱分析仪测量输出的毫米波噪声的频谱。

根据多光混频原理, 确定波长 $\lambda_1 = 1550.0 \text{ nm}$, 推导出其余五个具有不同中心波长 ($\lambda_2, \dots, \lambda_6$) 的

高斯型噪声光谱,中心波长分别为 1550.0, 1550.7, 1550.8, 1550.9, 1551.0, 1551.1 nm, 光谱如图 5(a)所示。由(2)式可知,当波长差 $\Delta\lambda$ (即 $\lambda_3 - \lambda_2$, $\lambda_4 - \lambda_3$, $\lambda_5 - \lambda_4$ 和 $\lambda_6 - \lambda_5$) 等于噪声光谱的半峰全宽时,在电噪声频谱中会产生 5 个高斯型频谱,其中心频率分别为 $f_1 = 87.5$ GHz, $f_2 = 100.0$ GHz,

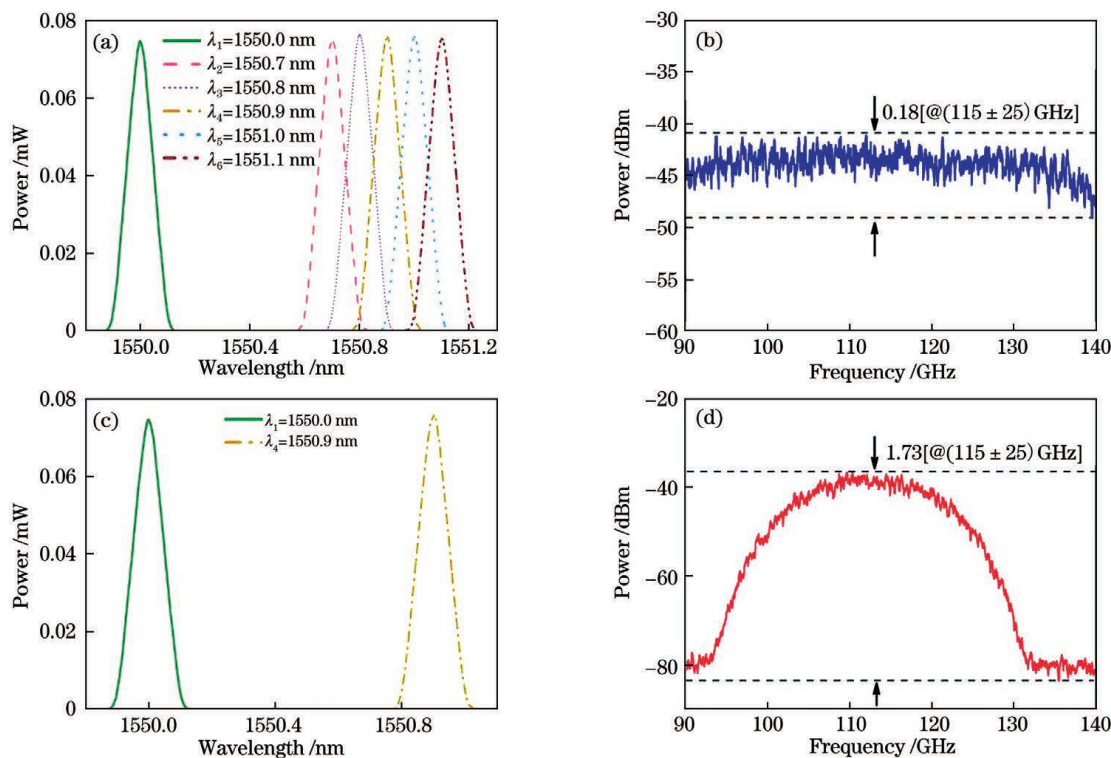


图 5 仿真结果。(a) 滤波后 6 个高斯型噪声光谱;(b) 多光混频的频谱;(c) 滤波后 2 个高斯型噪声光谱;(d) 双光混频的频谱

Fig. 5 Simulation results. (a) Six Gaussian noise spectra after filtering; (b) radio frequency spectrum output from mixing of multiple optical spectra; (c) two Gaussian noise spectra after filtering; (d) radio frequency spectrum output from mixing of two optical spectra

另外,进行了两个不同中心波长的高斯型噪声光谱混频的仿真,其波长差为 $\lambda_4 - \lambda_1$,对应频谱的中心频率为 $f_3 = 112.5$ GHz,其仿真结果如图 5(d)所示。通过计算,该方法得到的相对平坦度为 1.73 [@(115 ± 25) GHz]。显然,与双光混频的方法相比,我们提出的多光混频方法能够在 F 波段产生更平坦的毫米波噪声。

5 结 论

提出了一种基于多光混频产生平坦毫米波噪声的方法,并进行了模拟仿真与实验验证,证实了该方法的有效性。实验结果表明,该方法获得的电噪声谱的相对平坦度低至 0.46 [@(35 ± 15) GHz]。光电探测器的带宽决定生成电噪声的工作频段,因此在实验中使用了响应频段更高的光电探测器(如单

$f_3 = 112.5$ GHz, $f_4 = 125.0$ GHz 和 $f_5 = 137.5$ GHz,实验结果如图 5(b)所示。通过计算可知,相对平坦度为 0.18 [@(115 ± 25) GHz]。通过调整噪声光谱的波长、半峰全宽和数量等参数,所提方法也能够在 G 波段(140 ~ 220 GHz)内产生平坦的毫米波噪声。

行载流子光电探测器^[21]),该方法能够实现更大频率范围的平坦毫米波噪声的产生。由此可见,所提出的产生平坦毫米波噪声的方法在提高相关电子设备的测量能力方面具有较大潜力。

参 考 文 献

- [1] Lin J W, Lu C L, Chuang H P, et al. Photonic generation and detection of W-band chirped millimeter-wave pulses for radar[J]. IEEE Photonics Technology Letters, 2012, 24(16): 1437-1439.
- [2] Gopalsami N, Bakhtiari S, Elmer II T W, et al. Application of millimeter-wave radiometry for remote chemical detection[J]. IEEE Transactions on Microwave Theory and Techniques, 2008, 56(3): 700-709.
- [3] Choi K M, Baik J S, Lee C H. Broad-band light

- source using mutually injected Fabry-Pérot laser diodes for WDM-PON[J]. *IEEE Photonics Technology Letters*, 2005, 17(12): 2529-2531.
- [4] Isogawa T, Kumashiro T, Song H J, et al. Tomographic imaging using photonically generated low-coherence terahertz noise sources[J]. *IEEE Transactions on Terahertz Science and Technology*, 2012, 2(5): 485-492.
- [5] Ogut M, Bosch-Lluis X, Reising S C. A deep learning approach for microwave and millimeter-wave radiometer calibration[J]. *IEEE Transactions on Geoscience and Remote Sensing*, 2019, 57(8): 5344-5355.
- [6] Pepe D, Barnett C, D'Amore G, et al. On-chip millimeter-wave cold-source noise figure measurements with PNA-X[J]. *IEEE Transactions on Instrumentation and Measurement*, 2017, 66(12): 3399-3401.
- [7] Keen N J, Haas R W, Zimmerman P. Avalanche noise from Schottky barrier diodes in the frequency range 75–115 GHz (technical notes) [J]. *IEEE Transactions on Microwave Theory and Techniques*, 1978, 26(10): 843-844.
- [8] Arslan S, Yıldırım B S. A broadband microwave noise generator using Zener diodes and a new technique for generating white noise[J]. *IEEE Microwave and Wireless Components Letters*, 2018, 28(4): 329-331.
- [9] Coen C T, Frounchi M, Lourenco N E, et al. A 60-GHz SiGe radiometer calibration switch utilizing a coupled avalanche noise source[J]. *IEEE Microwave and Wireless Components Letters*, 2020, 30(4): 417-420.
- [10] Olsson N A. Lightwave systems with optical amplifiers [J]. *Journal of Lightwave Technology*, 1989, 7(7): 1071-1082.
- [11] Duan G H, Georgiev E. Non-white photodetection noise at the output of an optical amplifier: theory and experiment[J]. *IEEE Journal of Quantum Electronics*, 2001, 37(8): 1008-1014.
- [12] Song H J, Shimizu N, Furuta T, et al. Subterahertz noise signal generation using a photodetector and wavelength-sliced optical noise signals for spectroscopic measurements[J]. *Applied Physics Letters*, 2008, 93(24): 241113.
- [13] Shi J W, Kuo F M, Chiueh T, et al. Photonic generation of millimeter-wave white-light at W-band using a very broadband and high-power photonic emitter [J]. *IEEE Photonics Technology Letters*, 2010, 22(11): 847-849.
- [14] Song H J, Shimizu N, Kukutsu N, et al. Microwave photonic noise source from microwave to sub-terahertz wave bands and its applications to noise characterization[J]. *IEEE Transactions on Microwave Theory and Techniques*, 2008, 56(12): 2989-2997.
- [15] Sun J, Wu Y D, Wu W F, et al. Optimization of polarization-dependent loss of arrayed waveguide grating demultiplexer[J]. *Chinese Journal of Lasers*, 2020, 47(1): 0106003.
孙健, 吴远大, 吴卫锋, 等. 阵列波导光栅解复用器的偏振相关损耗的优化 [J]. *中国激光*, 2020, 47(1): 0106003.
- [16] Wang T, Chen H M, Jia H M, et al. Performance research and fabrication of 1310 nm superluminescent diodes with high power [J]. *Acta Photonica Sinica*, 2021, 50(6): 0623002.
王拓, 陈红梅, 贾慧民, 等. 1310 nm 高功率超辐射发光二极管的制备及性能研究 [J]. *光子学报*, 2021, 50(6): 0623002.
- [17] Derickson D. *Fiber optic test and measurement* [M]. Englewood Cliffs: Prentice-Hall, 1998: 169-220.
- [18] Nazarathy M, Sorin W V, Baney D M, et al. Spectral analysis of optical mixing measurements[J]. *Journal of Lightwave Technology*, 1989, 7(7): 1083-1096.
- [19] Vidal B. Broadband photonic microwave noise sources [J]. *IEEE Photonics Technology Letters*, 2020, 32(10): 592-594.
- [20] Qiao L J, Lü T S, Xu Y, et al. Generation of flat wideband chaos based on mutual injection of semiconductor lasers [J]. *Optics Letters*, 2019, 44(22): 5394-5397.
- [21] Zhen Z, Hao R, Xing D, et al. Nearly-ballistic optimization design of high-speed uni-traveling-carrier photodiodes[J]. *Chinese Journal of Lasers*, 2020, 47(10): 1006003.
甄政, 郝然, 邢东, 等. 高速单行载流子光电二极管的近弹道优化设计 [J]. *中国激光*, 2020, 47(10): 1006003.

Flat Millimeter-Wave Noise Generation Based on Mixing of Multiple Optical Spectra

Chen Yongxiang, Liu Wenjie, Sun Yuehui, Romain Zinsou, Wang Yuncai*

Guangdong Provincial Key Laboratory of Information Photonics Technology, School of Information Engineering, Guangdong University of Technology, Guangzhou, Guangdong 510006, China

Abstract

Objective In this paper, we propose a novel photonic method for generating flat millimeter-wave (mm-wave) noises. The principle of our method consists in reshaping the broadband amplified spontaneous emission (ASE) spectrum into a multiple Gaussian optical noise spectrum with different central wavelengths before beating on a wideband photo-detector (PD). For a better comparison of the quality of the generated noise, the relative flatness (γ) defined as the ratio of generated noise power fluctuation to its average power in a certain frequency range is put forward. The experimental results show that the relative flatness with the value of 0.46 [$@(35 \pm 15)$ GHz] is obtained by the proposed method. Benefitting from the low frequency-independent loss due to photonics devices, similar results can be achieved in higher frequency bands such as F-band (90–140 GHz) and G-band (140–220 GHz). This point is numerically confirmed.

Methods The aim of this paper is to improve the radio frequency (RF) spectral flatness of electrical noises generated by optically mixing multiple wavelength-sliced ASE lights. To do so, a broadband ASE spectrum from a superluminescent diode (SLD) source is reshaped into m narrowband Gaussian optical spectra using optical tunable filters with different central wavelengths ($\lambda_1, \lambda_2, \dots, \lambda_m$). Among them, the wavelength difference of λ_1 and λ_2 is adjusted to correspond to a desirable central frequency f_1 in the RF spectrum, and the difference between λ_1 and λ_m is adjusted to decide the expected central frequency f_{m-1} . At the same time, except λ_1 , the optical wavelength difference (i.e., $\lambda_3 - \lambda_2, \lambda_4 - \lambda_3, \dots, \lambda_m - \lambda_{m-1}$) between two consecutive spectra needs to be less than or equal to the 3 dB bandwidth of the optical tunable filter. In these conditions, the generation of the flat mm-wave noise in a frequency range of f_1 to f_{m-1} can be achieved. In addition, beating between the optical spectra centered at λ_2 to λ_m produces the electrical noise near the zero frequency region. This electrical noise component is neglected in this paper, because it is out of the target frequency range.

Results and Discussions According to Eqs. (3) and (4), it is demonstrated that the relative flatness of the noise signal is relevant to the number of optical spectra and full width at half maximum (FWHM) in F-band. The numerical simulation is performed assuming that the input optical power is maintained constant (Fig. 3). The optimal value of relative flatness is obtained when using six optical spectra and 0.1 nm FWHM. Due to the bandwidth limitation of the electrical devices such as the high-speed PD and electrical spectrum analyzer (ESA), we experimentally demonstrate the generation of the flat mm-wave noise in frequency range of 20 GHz to 50 GHz with a relative flatness of 0.46 [$@(35 \pm 15)$ GHz] using the mixing of multiple optical spectra [Fig. 4(b)]. In theory, the optical wavelength differences of $\lambda_1 - \lambda_2$ and $\lambda_1 - \lambda_3$ can produce two Gaussian electrical spectra with center frequencies of $f_1 = 25$ GHz and $f_2 = 37.5$ GHz. The RF spectral flatness improvement of the mm-wave noise is obtained due to the superimposition of these two Gaussian electrical noise spectra. For a better comparison, we also investigate the relative flatness in the mixing conditions of two optical spectra with central wavelengths of λ_1 and λ_3 [Fig. 4(d)]. It is noticed that the relative flatness is reduced to 0.65 [$@(35 \pm 15)$ GHz]. We can deduce that our proposed method enables a relative flatness improvement of about 0.19 [$@(35 \pm 15)$ GHz]. The simulation results relative to F-band noise generation using the proposed method are shown in Fig. 5. First, six optical noise spectra are applied to produce the mm-wave noise according to the Eqs. (3) and (4) with center wavelengths of $\lambda_1 = 1550.0$ nm, $\lambda_2 = 1550.7$ nm, $\lambda_3 = 1550.8$ nm, $\lambda_4 = 1550.9$ nm, $\lambda_5 = 1551.0$ nm, and $\lambda_6 = 1551.1$ nm, respectively [Fig. 5(a)]. Except for λ_1 , the differences between two consecutive optical spectra with $\lambda_3 - \lambda_2, \lambda_4 - \lambda_3, \lambda_5 - \lambda_4$, and $\lambda_6 - \lambda_5$ are all equal to the FWHM of the optical spectra. The mixing of six optical noise spectra generates Gaussian electrical noise spectra with central frequency of $f_1 = 87.5$ GHz, $f_2 = 100.0$ GHz, $f_3 = 112.5$ GHz, $f_4 = 125.0$ GHz, and $f_5 = 137.5$ GHz. Their superimposition yields a broadband electrical noise covering the frequency band of 90–140 GHz. It is obtained a relative flatness of 0.18 [$@(115 \pm 25)$ GHz] in F-band [Fig. 5(b)]. At the same time, the

case of two optical spectra mixing with center wavelengths of λ_1 and λ_4 is investigated [Fig. 5(c)]. The produced uneven electrical noise spectrum has a relative flatness of 1.73 [@(115 ± 25)GHz] [Fig. 5(d)]. In summary, our proposed method for optical mixing of multiple wavelength-sliced ASE signals can generate a flatter F-band mm-wave noise in comparison to that for optical mixing of two noise spectra.

Conclusions We theoretically and experimentally demonstrate the generation of flat millimeter-wave noises by optically mixing multiple Gaussian wavelength-sliced ASE lights. The proof-of-principle experiment has shown the effectiveness of our proposed method with a satisfactory relative flatness as low as 0.46 [@(35 ± 15)GHz]. Considering the non-dependency of fibers loss on frequency and the use of a photodetector with faster response such as uni-traveling-carrier photodiode (UTC-PD), the experimental implementation of our method in a higher frequency band can be expected. Our proposed method exhibits potential features for the noise parameter measurement of millimeter-wave devices.

Key words optical devices; flatness; millimeter-wave noise; mixing of multiple optical spectra; opto-electrical conversion